

EEGDM: EEG Representation Learning via Generative Diffusion Model

Jia Hong Puah, Sim Kuan Goh*, *Senior Member, IEEE*, Ziwei Zhang, Zixuan Ye, Chow Khuen Chan, Kheng Seang Lim*, Si Lei Fong, Kok Sin Woon, and Cuntai Guan, *Fellow, IEEE*

Abstract—While electroencephalogram (EEG) has been a crucial tool for monitoring the brain and diagnosing neurological disorders (e.g., epilepsy), learning meaningful representations from raw EEG signals remains challenging due to limited annotations and high signal variability. Recently, EEG foundation models (FMs) have shown promising potential by adopting transformer architectures and self-supervised pre-training methods from large language models (e.g., masked prediction) to learn representations from diverse EEG data, followed by fine-tuning on specific EEG tasks. Nonetheless, these large models often incurred high computational costs during both training and inference, with only marginal performance improvements as the model size increases. In this work, we proposed an EEG representation learning framework building upon Generative Diffusion Model (EEGDM). Specifically, we developed a structured state-space model for diffusion pretraining (SSMDP) to better capture the temporal dynamics of EEG signals and trained the model using a Denoising Diffusion Probabilistic Model. Subsequently, the resulting latent EEG representations were then used for downstream classification tasks via our proposed latent fusion transformer (LFT). To evaluate our method, we used multi-event datasets covering both interictal epileptiform discharges and seizure detection, and compared EEGDM with current state-of-the-art approaches, including EEG FMs. Empirical results showed that our method outperformed the existing methods. These findings suggested that EEGDM offered a promising alternative to current FMs. Our code is available at: <https://github.com/jhpuah/EEGDM>.

Index Terms—Electroencephalogram, diffusion model, representation learning, transformer, structured state-space model.

I. INTRODUCTION

LECTROENCEPHALOGRAPHY (EEG) provides a noninvasive technique for monitoring the brain by recording electrical signals arising from neural activity and pathological processes, with high temporal resolution. Its effectiveness has led to widespread use in brain–computer interfaces (BCIs), neuroscience research, and neurological diagnostics [1], [2]. A key clinical application is the management and treatment of epilepsy, which affects approximately 50 million patients worldwide [3], where EEG recognition plays a critical role in diagnosis and pre-surgical planning. Numerous machine learning and deep learning models have been developed to

detect interictal epileptiform discharges (IEDs) and seizures from EEG recordings, which often include various other brain activities (e.g., eye movements, artifacts, and other background activity). Despite showing initial promise, improving classification performance remains an active area of research for clinical adoption.

A major challenge behind the performance bottleneck in IED and seizure detection is the difficulty of learning robust and meaningful representations of EEG signals, due to limited high-quality annotation and high signal variability across subjects, conditions, and brain activities [2], [4]. Recently, inspired by the success of large language models (LLMs), various EEG foundation models (FMs) [4], [5] have been proposed and achieved different degrees of success. Following the procedure of LLMs, EEG FMs were pretrained on a large amount of unlabeled and diverse EEG data through self-supervised pre-training for representation learning using transformer architectures [6]. In most EEG FMs, the signals were tokenized into sequential tokens, with a subset masked to enable self-supervised training via masked token prediction [1], [2], [7]. These methods encouraged the models to learn the underlying relationships (through self- and cross-attention modules in the transformer) between tokens and effectively capture meaningful representations without relying on annotation. Subsequently, these FMs were fine-tuned on specific downstream tasks such as IED detection [2], sleep stage classification [8], and emotion recognition [9]. Although they often outperformed traditional deep learning models, they incurred high computational costs during both training and inference, with only marginal performance improvements as model size increased.

Diffusion models [10] represent another class of self-supervised learning and generative models that have demonstrated remarkable success in image [10], [11] and audio generation [12], [13]. Recent studies suggested that diffusion models also hold strong potential for representation learning tasks [14]. Unlike masking-based methods, diffusion models achieve self-supervision by progressively corrupting input data with Gaussian noise in a forward process and learning to recover the original data through a reverse denoising process. Several approaches [15]–[17] have been proposed to leverage diffusion models to extract representations for classification and segmentation of visual tasks. However, the generalization and applicability of diffusion models in EEG representation learning remain underexplored, as most existing works primarily employed them for signal generation and data augmentation [18]–[20], rather than for representation learning. Furthermore,

*Corresponding authors

J. H. Puah, S. K. Goh, Z. Zhang, Z. Ye were with the School of Artificial Intelligence and Robotics & J. H. Puah, K. S. Woon were with the School of Energy and Chemical Engineering, Xiamen University Malaysia.

C. K. Chan was with the Department of Biomedical Engineering & K. S. Lim, S. L. Fong were with the Department of Medicine, Universiti Malaya.

K. S. Woon was with the Thrust of Carbon Neutrality and Climate Change, Hong Kong University of Science and Technology (Guangzhou).

C. Guan was with the College of Computing & Data Science, Nanyang Technological University.

it is also unclear whether the learned representation would be useful and how to use it for downstream classification tasks. Hence, this work attempts to fill this gap.

In this work, we propose an EEG Representation Learning Framework, building upon the Generative Diffusion Model (EEGDM). Specifically, we developed a neural architecture based on a structured state-space model for diffusion pre-training (SSMDP) to better capture the temporal dynamics of EEG signals and trained the architecture using a Denoising Diffusion Probabilistic Model (DDPM). Subsequently, the resulting latent EEG representations were then used for downstream classification tasks via our proposed latent fusion transformer (LFT). To evaluate our method, we used the Temple University EEG Event Corpus (TUEV) [21] and Children’s Hospital Boston-Massachusetts Institute of Technology (CHB-MIT) [22], which contained IED and seizure, respectively, and compared EEGDM with current state-of-the-art approaches, including EEG FMs.

The main contributions of this work are as follows:

- We presented EEGDM, a diffusion model-based framework for learning EEG signal representations and classification of multi-event EEG, extending diffusion model beyond signal generation and data augmentation.
- We developed SSMDP to capture the temporal dynamics of EEG signals and trained it via the forward and reverse process of DDPM for representation learning using TUEV dataset.
- We proposed LFT to leverage and integrate the latent representations learned by SSMDP for downstream tasks, including TUEV (seen during pretraining) and CHB-MIT (unseen during pretraining) datasets.
- We empirically compared our method with state-of-the-art on TUEV and CHB-MIT, and provided a detailed ablation study to analyze its components.

II. RELATED WORKS

This section reviews the evolution of EEG representation learning, from classical supervised, unsupervised, and semisupervised approaches to recent advances in self-supervised learning (particularly FMs and diffusion models) and their emerging potential for EEG, with an emphasis on the latter.

A. Supervised and Unsupervised Approaches

EEG representation learning has often arisen as a byproduct of supervised approaches, such as the seminal common spatial pattern methods [23] and more recent deep neural network models [24]. Such representations have been examined across various neural architectures, including convolutional neural networks [25], graph neural networks [26], [27], and Transformers [28], [29], revealing findings that aligned with known brain activity patterns. When annotations are unavailable, unsupervised approaches, particularly autoencoders and their variants, offered an alternative. Variational autoencoder (VAE) has shown effectiveness in learning robust representation in the regularized latent space, achieving transfer learning from motor execution signal to motor imaginary signals [30]. Another approach was metric learning, which embedded EEG signals

into a vector space where similarity was defined as proximity between samples, typically optimized using contrastive loss (e.g., [31]). However, these methods are constrained by the availability of annotation and often yield task-specific representations that lack generalizability.

Another line of research was semi-supervised learning that leverages a small amount of annotated data to train a model, while using the model itself to generate “pseudo-labels” for unannotated data, which can then be used as additional training data. For example, in [32], the empirical probabilities of the training data are used as pseudo-labels to calibrate model certainty and confidence, thereby addressing the scarcity of annotations in motor imagery classification. Another promising approach was self-supervised learning, which learns by corrupting and subsequently restoring the training data. Common corruption strategies included masking, adding noise, or combining both. These techniques have been successfully applied to various EEG tasks, such as sleep stage classification [33], evoked response enhancement [34], and motion intention recognition [35]. Recently, self-supervised pretraining methods, particularly mask prediction with transformers and diffusion models, have demonstrated strong potential across multiple domains. However, only a few pioneering studies have begun to explore their effectiveness in EEG representation learning.

B. EEG FMs

Inspired by LLMs, EEG FMs employed token-based and masking-based self-supervised pretraining on a diverse and large amount of unannotated data with transformer architectures before finetuning the pretrained model with annotation in a supervised manner. The pre-training allowed EEG FMs to grasp the underlying structure of EEG from various problem domains and experimental paradigms, thus addressing the annotation scarcity issue and reducing the risk of overfitting [36]. Prior to pre-training, the raw EEG signal was usually preprocessed and then segmented into patches. A tokenizer, usually a variant of vector-quantized (VQ) VAE [37], was trained to encode these patches into discrete representations, known as tokens. The VQ encoder first projected a patch to a vector representation, then the representation was replaced by the most similar entry (token) from a codebook. The VQ decoder then reconstructed a target from the token, either the original patch itself (in CBraMod [6] and Gram [7]) or a transformation of the original patch, such as Fourier spectrum (in LaBraM [2]). This process ensured that the tokens in the codebook capture semantically meaningful information about the original patches.

Subsequently, self-supervised pretraining operates on the sequence tokenized by the VQ encoder and the codebook. Initially, a subset of a sequence is masked by randomly replacing some of the tokens with a “mask token”. The masked sequence is then processed by a transformer-based model to predict the index of the replaced tokens in the codebook. The neural architecture of the model varies: LaBraM [2] used a classic transformer, CBraMod [6] employed a criss-cross attention mechanism to model spatial and temporal dependencies in parallel, and Gram [7] used a masked autoencoder

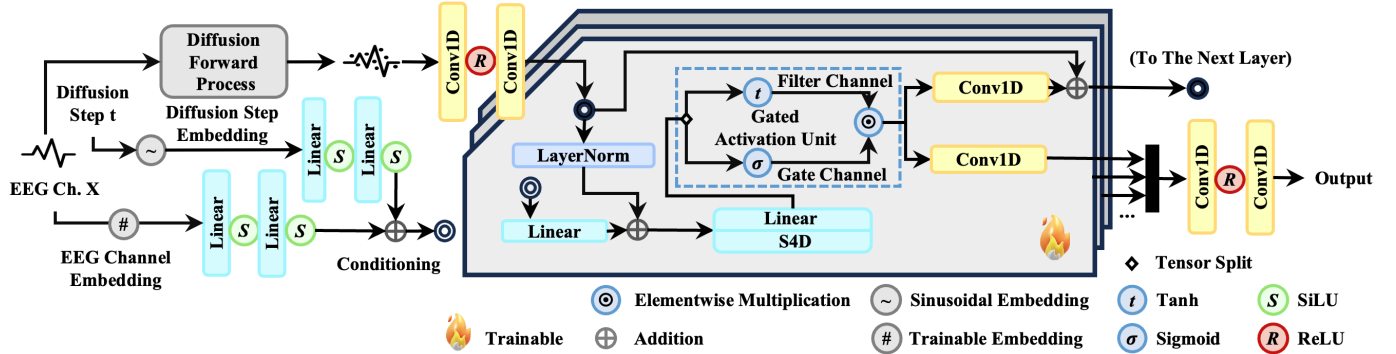


Fig. 1. Illustration of the proposed SSMDP for representation learning. The model learned to denoise and reverse a noised single-channel EEG signal by predicting the diffusion velocity, conditioned on diffusion step embedding and channel embedding, using S4D architecture. The latent activities from the gate or filter channels were then leveraged for downstream classification.

consisting of a layer-fusion encoder and a transformer-based decoder. Subsequently, the pretrained model can be finetuned for classification tasks. Usually, a trainable “class token” is concatenated into the input sequence to be processed by transformer. Then, a linear classification head was trained to classify the processed class token to a label. While EEG FMs often outperformed classical deep learning models, they incurred high computational costs during both training and inference, with only marginal performance improvements as model size increases.

C. Diffusion Model in Representation Learning

Diffusion models are closely related to denoising autoencoders [38], which are capable of producing meaningful representations in their latent space. In particular, denoising diffusion autoencoder [14] showed that the inner working of diffusion models was analogous to an autoencoder. Several works explored the efficiency of latent activities of diffusion models in image classification [16], [17] and image segmentation task [15].

In addition to latent activities, the connection between conditional diffusion models and conditional probability distributions also led to alternative ways in representation learning. Diffusion classifier [39] showed that any conditional diffusion model can be converted into a classifier without additional training. Joint diffusion model [40] unified this generator-classifier duality: the model was explicitly trained to minimize both classification loss and generative loss, so it can perform both tasks in a single model. These findings presented a promising direction for generalization to EEG representation learning and classification tasks, despite being underexplored.

D. Diffusion Models for EEG Signals

There is limited work on adapting diffusion models to EEG signal representation learning. Early works have primarily used EEG signals as conditioning inputs to generate other modalities, such as images [41] and audio [42], rather than learning representations of the EEG itself. A more relevant line of research [43], [44] integrates diffusion models within an autoencoder framework, so that the reconstruction errors from

the diffusion model can help formulate a more informative latent space, thereby enhancing performance in imagined speech classification [43] and driving behavior classification [44]. Inspired by image super-resolution (e.g. [45]), [46] proposed a diffusion model that can generate high-resolution EEG from low-resolution EEG, to migrate the data scarcity issue for downstream classification task and improve spatial resolution for signal source localization. [47] applied a conditional diffusion model to generate a clean EEG signal under the guidance of noisy EEG signals, hence suppressing EEG artifacts such as electrooculography artifacts.

Several works [18]–[20] quantitatively evaluated the similarity between the generated and real signals, and used the synthesized data for augmentation in various downstream tasks, such as imagined motor activity detection and major depressive disorder classification. Nonetheless, the generalization and applicability of diffusion models in EEG representation learning remain underexplored. Moreover, the optimal strategies for leveraging the learned representations are still unclear. These open questions motivate the present work.

III. METHODOLOGY

We first present the preliminaries of key components (diffusion models, state-space models, and transformers) that EEGDM builds upon, followed by our EEGDM.

A. Preliminaries

1) *Diffusion Model*: A diffusion model consists of a forward process and a reverse process. The forward process gradually transforms a target data distribution into a standard Gaussian distribution, while the reverse process learns to denoise step by step to reconstruct the original data. After training, the reverse process can be used for generation by gradually transforming a sample from the Gaussian distribution into one that resembles the target data distribution.

The forward process models the trajectory of a data point \mathbf{x}_0 drifts and diffuses from its original distribution $p(\mathbf{x}_0)$ to the Gaussian distribution $\mathcal{N}(0, I)$. This process is split into T diffusion steps, where each step is an intermediate distribution dependent on the original data and a noise schedule $\bar{\alpha}$:

$$p(\mathbf{x}_t | \mathbf{x}_0) = \sqrt{\bar{\alpha}_t} \mathbf{x}_0 + \sqrt{1 - \bar{\alpha}_t} \epsilon \quad (1)$$

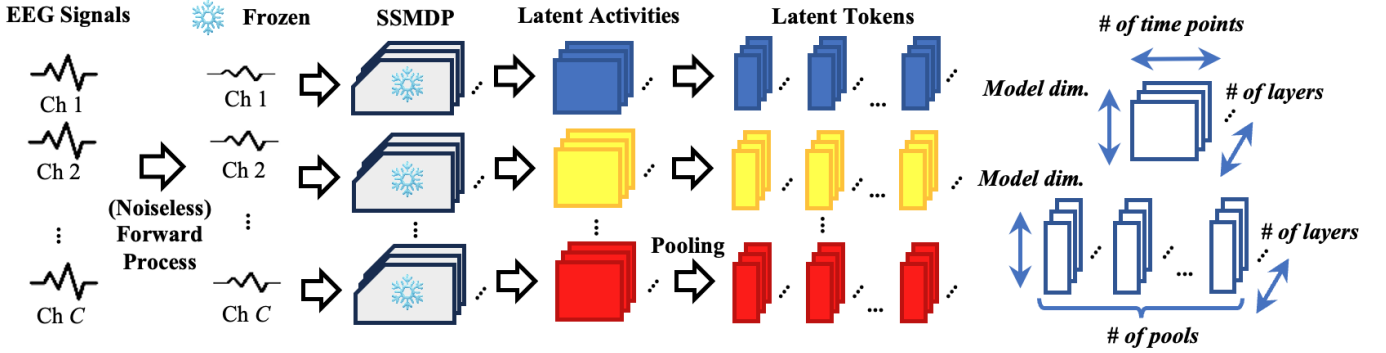


Fig. 2. From the pretrained SSMDP, we obtain the latent activities of each EEG channel as a four-dimensional tensor: (# of channels, # of layers, # of time points, # of gate channels per layer). The latent activities are then pooled along the time dimension, reducing the dimensionality to (# of channels, # of layers, # of pools, # of gate channels per layer). Colors indicate the latent activities from different channels.

where $t = 1, 2, 3 \dots, T$, $\epsilon \sim \mathcal{N}(0, I)$, and $\bar{\alpha}_t \in (0, 1)$ is a set of strictly decreasing hyperparameters controlling the noise schedule.

The reverse process starts from a pure Gaussian distribution $q(\mathbf{x}_T)$. The model is trained to perform denoising under the assumption that each transition step in the reverse process is also Gaussian. This assumption becomes increasingly valid as the number of diffusion steps T grows large. The reverse process is modeled as:

$$q_\theta(\mathbf{x}_{t-1} | \mathbf{x}_t) = \mathcal{N}(\mathbf{x}_{t-1}; \mu(\mathbf{x}_t, t), \sigma_t^2) \quad (2)$$

parameterized by mean μ and variance σ_t^2 . σ_t^2 is assumed to be a function of $\bar{\alpha}_t$ and not dependent on \mathbf{x}_t . Previous works have found that, instead of predicting μ , predicting added noise [10] or velocity [48]:

$$v_t = \sqrt{\bar{\alpha}_t} \epsilon - \sqrt{1 - \bar{\alpha}_t} \mathbf{x}_0 \quad (3)$$

gives better results in general.

A deep neural network Φ is trained to approximate the chosen target v_t with a training loss \mathcal{L} to maximize the evidence lower bound of $q_\theta(\mathbf{x}_0)$, which is typically simplified to minimize the mean square error (MSE) between the prediction and the actual target of every diffusion step [10]:

$$\mathcal{L}_{\text{MSE}} = \mathbb{E}_{t \sim [1, T]} [\|v_t - \Phi(\mathbf{x}_t, t)\|^2] \quad (4)$$

Diffusion models do not have restrictions on the architecture of the backbone model Φ , some popular choices include U-Net [49] and transformer [50]. Conditional diffusion models accept additional inputs c known as “conditioning” that provide supplementary information about the target \mathbf{x}_0 , such as its class label. This effectively converts the outcome of the reverse diffusion process into conditional distributions $q_\theta(\mathbf{x}_0 | c)$, allowing for a finer control over the generation outcome [51].

2) *Structured State-Space Model*: Structured state-space models [52] (SSMs) are a class of neural networks that originate from the state-space representation of a dynamic system in control theory. SSMs project a continuous-time input

$x(\tau)$ to a continuous-time output $y(\tau)$ and a hidden state $h(\tau)$ with matrices $\mathbf{A}, \mathbf{B}, \mathbf{C}$ and \mathbf{D} :

$$\mathbf{h}'(\tau) = \mathbf{A}h(\tau) + \mathbf{B}x(\tau) \quad (5a)$$

$$y(\tau) = \mathbf{C}h(\tau) + \mathbf{D}x(\tau) \quad (5b)$$

In practice, continuous-time data are often unavailable, so SSMs are typically computed using their discrete-time approximations:

$$h_k = \bar{\mathbf{A}}h_{k-1} + \bar{\mathbf{B}}x_k \quad (6a)$$

$$y_k = \mathbf{C}h_k + \mathbf{D}x_k \quad (6b)$$

The matrices in Eq. (6a) can be trained directly or obtained by applying a discretization rule with trainable step size Δ on Eq. (5a), like zero-order hold:

$$\bar{\mathbf{A}} = \exp(\Delta \mathbf{A}), \quad \bar{\mathbf{B}} = (\Delta \mathbf{A})^{-1}(\exp(\Delta \mathbf{A} - I))(\Delta \mathbf{B}) \quad (7)$$

This approach preserves the continuous-time structure of SSMs, enabling the model to operate at different sampling rates without retraining through the adjustment of Δ [52]. However, in practice, this advantage may be diminished if the SSM is used alongside components that are inherently dependent on the sampling rate.

Unrolling the formulae in Eq. (6) will eliminate h_k , which results in the convolution form of SSMs that can be trained efficiently:

$$\begin{aligned} \bar{\mathbf{K}} &= (\bar{\mathbf{C}}\bar{\mathbf{B}}, \bar{\mathbf{C}}\bar{\mathbf{A}}\bar{\mathbf{B}}, \bar{\mathbf{C}}\bar{\mathbf{A}}^2\bar{\mathbf{B}}, \dots, \bar{\mathbf{C}}\bar{\mathbf{A}}^{L-1}\bar{\mathbf{B}}) \\ y &= \bar{\mathbf{K}} * x = \sum_{i=0}^k \bar{\mathbf{C}}\bar{\mathbf{A}}^i\bar{\mathbf{B}}x_{k-i}, \quad k = 0, \dots, L-1 \end{aligned} \quad (8)$$

However, in practice, the calculation of $\bar{\mathbf{A}}^i$ in Eq. (8) is a performance bottleneck and is vulnerable to the vanishing gradient problem. The S4D [53] overcomes this by constraining \mathbf{A} to be a diagonal matrix with special initialization schemes.

3) *Transformer*: Transformers [50] are a class of neural networks that implement attention mechanisms. The attention mechanisms learn the dependencies between two sequences of tokens $\mathbf{S}_1 \in \mathbb{R}^{L_1 \times H_1}$ and $\mathbf{S}_2 \in \mathbb{R}^{L_2 \times H_2}$ and produce a new sequence with the same dimensions as \mathbf{S}_1 . Here, L_i denotes the length of the sequence and H_i denotes the dimension of

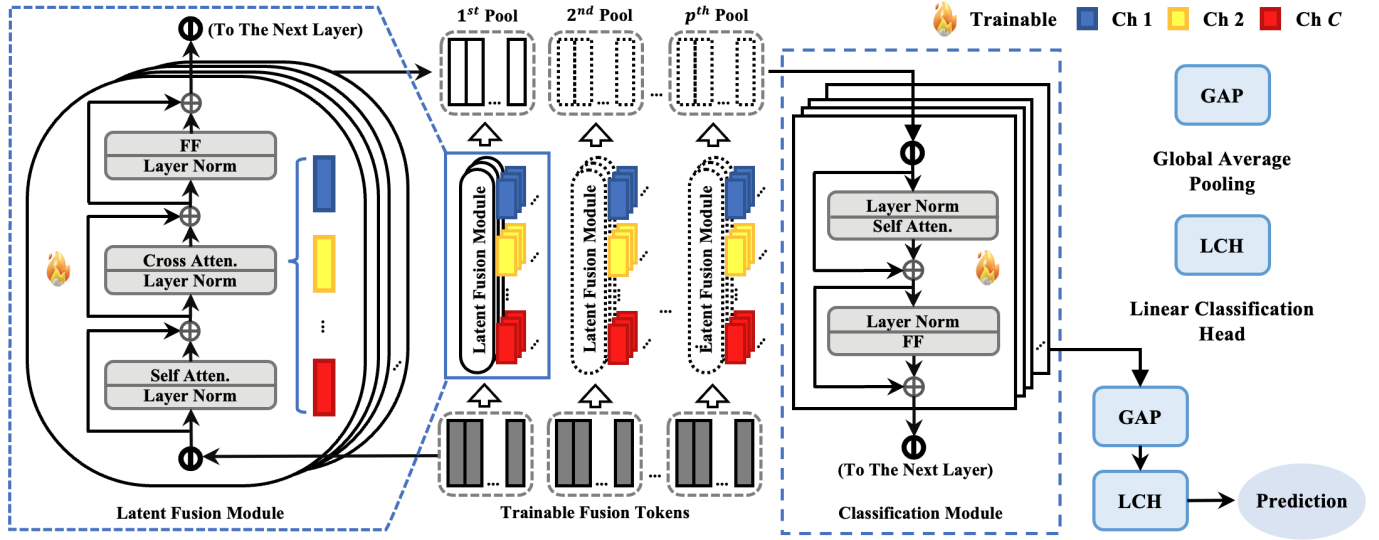


Fig. 3. Architecture of the proposed LFT. LFT comprises two main modules: latent fusion and classification modules. Left: The latent fusion module processes tokens from one pool at a time, with each block handling tokens from a single layer. Trainable fusion tokens are passed sequentially between blocks, integrating nonisomorphic representations from different layers via cross-attention. Middle: To capture time-invariant representations, the same fusion model is applied to every pool. Right: The classification module fused representations from all pools. Subsequently, LFT applies global average pooling followed by a linear classification head to generate predictions.

a token. If $S_1 = S_2$, the attention mechanism is termed “self attention”, otherwise, it is termed “cross attention”.

In the attention mechanism, each token of input sequences is first linearly projected to a subspace with dimension H to obtain query \mathbf{Q} , key \mathbf{K} , and value \mathbf{V} matrices:

$$\begin{aligned} \mathbf{Q} &= \mathbf{S}_1 \mathbf{W}_Q, \quad \mathbf{K} = \mathbf{S}_2 \mathbf{W}_K, \quad \mathbf{V} = \mathbf{S}_2 \mathbf{W}_V \\ \mathbf{Q} &\in \mathbb{R}^{L_1 \times H}, \quad \mathbf{K}, \mathbf{V} \in \mathbb{R}^{L_2 \times H} \end{aligned} \quad (9)$$

$$\text{Attention}(\mathbf{Q}, \mathbf{K}, \mathbf{V}) = \text{softmax} \left(\frac{\mathbf{Q} \mathbf{K}^T}{\sqrt{H}} \right) \mathbf{V}$$

The attention mechanism produces a new matrix with the same dimension as \mathbf{Q} . Each row in this new matrix is a different weighted average of the rows in \mathbf{V} , where the weight is divided by the scaled dot product between the corresponding row in \mathbf{Q} and all rows in \mathbf{K} . This is similar to a simplified cosine similarity, with the denominator replaced by a constant. Through the attention mechanism, information from different parts of \mathbf{V} can be dynamically selected and routed to different parts of the output.

Multi-head attention (MHA) is a commonly used variation of the attention mechanism. In MHA, attention is calculated on h different sets of \mathbf{Q} , \mathbf{K} , and \mathbf{V} , then the outputs are concatenated and linearly projected back to the desired dimension.

$$\begin{aligned} \mathbf{h}_i &= \text{Attention}(\mathbf{Q}_i, \mathbf{K}_i, \mathbf{V}_i) \\ \text{MHA}(\mathbf{Q}, \mathbf{K}, \mathbf{V}) &= [\mathbf{h}_1 \quad \mathbf{h}_2 \quad \mathbf{h}_3 \quad \dots \quad \mathbf{h}_h] \mathbf{W}_O \end{aligned} \quad (10)$$

B. EEGDM

Building upon the aforementioned components, EEGDM comprises two main modules: (1) SSM-Based Diffusion Pre-training (SSMDP) for EEG representation learning, and (2) LFT for downstream classification tasks. We detail the neural architectures and training procedures of each component in the following subsections.

1) *SSM-Based Diffusion Pretraining*: Our diffusion pre-training module was built upon SSMs, which were designed to capture the temporal dynamics of EEG signals. EEG signals were first subjected to a forward diffusion process, progressively injecting noise into the signals. Our model then learned to reverse this process step by step, denoising the input and learning meaningful latent representations. The architecture preserved fine-grained temporal structures while capturing long-range dependencies across time steps.

A known limitation of SSMs was their unidirectional nature: they model each output y_k as a function of current and past inputs $x_{0:k}$, while completely ignoring future inputs $x_{k+1:L}$. To model bidirectional dependencies, we adopt a dual-SSM setup, wherein one SSM processes the original sequence in the forward direction and another processes the reversed sequence, as suggested in previous work [13]. SSMDP is illustrated in Fig. 1. In this work, SSMDP consisted of 20 layers of SSMs, each layer contained 128 gate channels and 128 filter channels. Each channel, either gate or filter, had its own trainable bidirectional SSM with 128-dimensional hidden state. The SSMs were initialized with diag-lin scheme (see [53]).

SSMDP processed signals from each EEG channel individually, and twenty-two 128-dimensional trainable channel embeddings were included to encode the spatial context of input signals, corresponding to the 22 EEG channels that appear in TUEV, while the diffusion step was embedded through sinusoidal embedding [50]. The sum of these two embeddings is fed to the backbone model as conditioning, informing the model about the differences in spatial coordinate and noise level.

2) *Latent Fusion Transformer*: The LFT employed a transformer-based architecture to integrate latent activities from the gate or filter channels generated by the SSMDP, illustrated in Fig. 3. Gate channels were selected based on

empirical analysis (see Section V-B2). Due to the large dimensionality of the latent activities, subsequent processing became computationally demanding. Here, the diffusion backbone used in our setup produces latent activities with a dimensionality 2560 times larger than the original input (20 layers \times 128 gate channels). To reduce this burden, the latent activities were pooled based on windowing (e.g., average and standard deviation pooling), illustrated in Fig. 2.

Subsequently, a decoder-only transformer named the latent fusion module aggregated the SSM latent representations into a structured sequence. We defined latent fusion tokens that are prepended to the per-channel and per-pool latent representations, and the transformer’s self-attention mechanism jointly processed the sequence, enabling the modeling of inter-channel and inter-pool dependencies and fusion into context-aware features. These fused representations were then passed to the classification module, an encoder-only transformer, which captured inter-token dependencies, and followed by a linear classification head with softmax activation.

The LFT implemented had 20 decoder blocks in the latent fusion module and 8 encoder blocks in the classification module, each equipped with 8-headed attention. The embedding dimension of the attention mechanism was 128, and the hidden dimension of the multilayer perceptron was 512.

3) Training Procedures:

a) *Signal Embedding*: EEG data exhibit a wide dynamic range with occasional extreme values, which can hinder model training. To address this, we apply the μ -law companding:

$$u(x) = \begin{cases} \text{sgn}(x) \frac{\ln(1+\mu|x|)}{\ln(1+\mu)}, & \text{if } |x| > 1 \\ x, & \text{otherwise.} \end{cases} \quad (11)$$

where x denotes the normalized signal and $\mu = 255$. This non-linear transformation compressed the large-amplitude values more than the smaller ones, effectively suppressing outliers and enhancing numerical stability. In addition to signal embedding, we included learnable embeddings for EEG channels and sinusoidal embeddings for diffusion timesteps to provide spatial and noise-level context to the model, as shown in Fig. 1.

b) *Pretraining of SSMDP*: We adopted DDPM and modified the noise schedule as EEG signals are approximately Gaussian-distributed [54] and typically exhibit low signal-to-noise ratios. To preserve signal integrity across diffusion steps, we adopt a less aggressive noise injection scheme compared to standard DDPM configurations. Specifically, the total diffusion timestep T was set to 50 (in contrast to the typical 1000), and we employed the cosine noise schedule [11].

c) *Fine-tuning of LFT*: During fine-tuning, each EEG channel was processed by SSMDP, and the *latent activities* from all gate channels across all layers were collected.

As illustrated in Fig. 2, given an EEG segment with C channels and L samples, processed by a backbone model with n layers and H gate channels, the resulting latent activities form a tensor of shape (C, n, L, H) . We divided the time axis (L) into p segments and performed pooling, yielding latent tokens with shape (C, n, p, H) . The gate dimension H serves as the embedding dimension, so each token summarizes latent activity within a local window of L/p samples for a specific channel and layer.

Latent fusion was performed using a decoder-only transformer (Fig. 3). For each temporal pool, there were n groups of C latent tokens (each of dimension H) that represented activity across EEG channels. Since each group encoded different information, we assign a dedicated decoder block to each group. N trainable latent fusion tokens were sequentially passed through these decoder blocks: first through the block for the first group, then the second, and so on. Within each decoder block, the fusion tokens acted as queries, and the corresponding latent tokens served as keys and values. This design condensed the C -channel information into N context-rich fusion tokens for each temporal pool. In this work, $C = 22$, $n = 20$, $L = 1000$, $H = 128$, and $N = 16$. p was the number of seconds in the EEG segment, which is 5 for TUEV and 10 for CHB-MIT.

The resulting fusion tokens from all p temporal pools were concatenated and passed to an encoder-only transformer (Fig. 3). This transformer captured dependencies across pools and fusion tokens. Then, its outputs were global average-pooled and fed into a linear classification head. The classification module was trained in a supervised manner, representing the fine-tuning phase of the EEGDM framework.

IV. EXPERIMENT

The experimental details include: (1) dataset preprocessing, (2) training configurations and hyperparameters, and (3) evaluation methodology and baseline comparisons.

A. Dataset Preprocessing

The TUEV [21] dataset is a multi-event dataset from the TUH EEG Corpus [55] for the detection and classification of epileptic events from EEG recordings, including other brain activities such as eye movements, artifacts, and background. The recordings were sampled at a 250 Hz sampling rate and referenced using a transverse central parietal (TCP) montage. The recordings in the dataset were labelled with the following annotations: spike and slow wave (SPSW), generalized periodic epileptiform discharge (GPED), periodic lateralized epileptiform discharge (PLED), eye movement (EYEM), artifact (ARTF), and background (BCKG).

We followed the same preprocessing steps of LaBraM [2] and NeuroLM [5]: 0.1 Hz - 75 Hz band pass filtering with a 50 Hz notch filter, resampling to 200 Hz, and finally scaling down the signal amplitude (in μ V) by 100 to ensure that most values are between -1 and 1. The recordings were then segmented into 5-second samples. The training data were divided into two sets, 80% training set and 20% validation set.

B. Training Configurations and Hyperparameters

The SSMDP was trained with a batch size of 108 for 100 epochs using the AdamW optimizer. The prediction target was velocity (see Eq. (3)). The learning rate, weight decay, β_1 , and β_2 were 10^{-4} , 0, 0.99, and 0.999, respectively. An exponential moving average (EMA) was applied to the model with a decay rate of 0.999. Gradients were clipped by their norm with a threshold of 1. The model size of SSMDP was 5.9M parameters.

TABLE I
COMPARATIVE ANALYSIS (%) ON MULTI-EVENT TUEV WITH FMs AND NON-FMs.

Model	Size	Kappa	BAcc	WF1
<i>Training from Scratch (non-FM)</i>				
SPaRCNet [56]	0.79M	42.33 \pm 1.81	41.61 \pm 2.62	70.24 \pm 1.04
ContraWR [57]	1.6M	39.12 \pm 2.37	43.84 \pm 3.49	68.93 \pm 1.36
FFCL [58]	2.4M	37.32 \pm 1.88	39.79 \pm 1.04	67.83 \pm 1.20
CNN-Trans [59]	3.2M	38.15 \pm 1.34	40.87 \pm 1.61	68.54 \pm 2.93
ST-Trans [60]	3.5M	37.65 \pm 3.06	39.84 \pm 2.28	68.23 \pm 1.90
<i>Fine-tuning of Pretrained Parameters (FM)</i>				
BIOT [1]	3.2M	52.73 \pm 2.49	52.81 \pm 2.25	74.92 \pm 0.82
LaBraM-Base [2]	5.8M	64.33 \pm 0.87	67.25 \pm 1.02	82.01 \pm 0.87
LaBraM-Large [2]	46M	66.22 \pm 1.36	65.81 \pm 1.56	83.15 \pm 0.40
LaBraM-Huge [2]	369M	66.80 \pm 1.85	66.95 \pm 1.54	84.01 \pm 0.38
CBraMod [6]	4.0M	67.72 \pm 0.96	66.71 \pm 1.07	83.42 \pm 0.64
Gram-B [7]	6.0M	65.28 \pm 1.79	73.26 \pm 0.93	86.14 \pm 0.80
Gram-M [7]	47.19M	66.77 \pm 2.27	74.06 \pm 1.26	86.74 \pm 1.17
Gram-L [7]	251.28M	71.30 \pm 3.33	74.87 \pm 1.51	88.24 \pm 1.58
<i>Freezing of Pretrained Parameters (FM)</i>				
MMM [9]	0.36M	23.22 \pm 1.55	52.69 \pm 0.71	68.20 \pm 1.93
BENDR [8]	157.14M	39.64 \pm 1.48	50.09 \pm 2.24	75.35 \pm 1.07
EEGPT-Tiny [4]	4.7M	50.85 \pm 1.73	56.70 \pm 0.66	75.35 \pm 0.97
EEGPT [4]	25M	63.51 \pm 1.34	62.32 \pm 1.14	81.87 \pm 0.63
NeuroLM-B [5]	254M	42.85 \pm 0.48	45.60 \pm 0.48	71.53 \pm 0.28
NeuroLM-L [5]	500M	44.14 \pm 9.96	41.32 \pm 12.35	73.87 \pm 4.00
NeuroLM-XL [5]	1696M	45.70 \pm 4.98	46.79 \pm 3.56	73.59 \pm 2.19
<i>Freezing of Pretrained Parameters (non-FM)</i>				
EEGDM (Ours)	12.8M	74.23 \pm 1.36	75.57 \pm 1.47	86.88 \pm 0.66

The LFT was trained using the cross-entropy loss function, regularized with a label smoothing factor of 0.1. A batch size of 256 was used, evenly distributed across the available GPUs. The AdamW optimizer was employed with a weight decay of 0.05, and momentum parameters $\beta_1 = 0.9$ and $\beta_2 = 0.98$. No layer-wise parameter tuning was applied; therefore, the learning rate and weight decay were kept uniform across all layers. Latent fusion tokens and bias terms were exempted from weight decay. The initial learning rate was set to 10^{-5} and scheduled using a one-cycle cosine annealing policy, with a peak learning rate of 5×10^{-4} and a warm-up period of 5 epochs. To stabilize training, an exponential moving average was applied with a decay rate of 0.999. Additionally, gradients were clipped by their global norm, with a threshold of 3. The model size of LFT was 6.9M parameters.

The LFT was trained for a maximum of 50 epochs, with early stopping applied if the validation Cohen's kappa score did not improve for at least 3 consecutive epochs after epoch 20. Following training, the checkpoint with the highest validation score was selected for evaluation in the test set. The experiments were conducted on a server equipped with Intel Xeon CPUs and eight NVIDIA GeForce RTX 4090 GPUs.

C. Evaluation and Baselines

The classification performance was evaluated using balanced accuracy ("BAcc"), Cohen's kappa ("kappa"), and weighted F1 score ("WF1"). We reported the mean and

TABLE II
ABLATIONS OF μ -LAW, NOISE SCHEDULER AND NOISELESS FORWARD PROCESS (%)

Model Setting	Kappa	BAcc	WF1
EEGDM	74.23 \pm 1.36	75.57 \pm 1.47	86.88 \pm 0.66
- μ -law Signal Embedding	72.50 \pm 3.02	69.12 \pm 1.81	85.79 \pm 1.41
- Cosine Noise Schedule	70.97 \pm 1.04	71.19 \pm 0.92	85.07 \pm 0.49
- Noiseless Forward Process	71.39 \pm 1.46	56.19 \pm 3.34	84.87 \pm 0.54

TABLE III
IMPACTS OF DIFFERENT DIFFUSION TIME STEP (%)

Step	Kappa	BAcc	WF1
No	74.23 \pm 1.36	75.57 \pm 1.47	86.88 \pm 0.66
1	74.46 \pm 1.39	<u>74.87 \pm 1.83</u>	86.94 \pm 0.68
2	73.73 \pm 1.16	74.83 \pm 1.55	86.66 \pm 0.55
3	69.05 \pm 1.63	69.89 \pm 1.49	84.34 \pm 0.81

TABLE IV
IMPACTS OF POOLING STRATEGIES AND LATENT ACTIVITIES

Pool	Latent	Kappa	BAcc	WF1
Std	Gate	74.23 \pm 1.36	75.57 \pm 1.47	86.88 \pm 0.66
Std	Filter	<u>73.46 \pm 2.33</u>	<u>68.74 \pm 0.63</u>	<u>86.49 \pm 1.18</u>
Mean	Gate	71.66 \pm 1.13	57.71 \pm 1.89	85.24 \pm 0.57
Mean	Filter	69.83 \pm 1.92	68.33 \pm 3.17	84.46 \pm 1.05

standard deviation of performance across five independent runs. The selected baselines include deep learning models trained from scratch (SPaRCNet [56], ContraWR [57], FFCL [58], CNN-Trans [59], and ST-Trans [60]) and EEG FMs (MMM [9], BENDR [8], BIOT [1], EEGPT [4], LaBraM [2], CBraMod [6], Gram [7], and NeuroLM [5]).

V. RESULTS & DISCUSSION

We evaluated our model on the multi-event TUEV EEG classification task and compared its performance against several strong baselines, including those trained from scratch, EEG FMs that involved a pre-training stage. In addition, we conducted ablation studies to investigate the contributions of key components in EEGDM, such as input noising strategies, latent activity extraction methods, the hierarchical structure captured in the learned latent representations, and latent fusion mechanisms. Moreover, we examined the model's ability to generalize to another EEG dataset (CHB-MIT [22]) as well as EEG data sampled from different frequencies. A sample of EEG generated by SSMDP can be found on our GitHub.

A. Main Results

In Table I, we report the mean and standard deviation of "kappa", "BAcc", and "WF1", averaged over five runs with different random seeds, trained on a single dataset (non-FM) vs. pretrained on multiple datasets (FM). Detailed model sizes were also provided. In general, FMs exhibited a scaling law, with performance improving as model size increased. Furthermore, FMs that fine-tuned pre-trained parameters typically outperformed those that froze them for efficiency. However,

TABLE V
IMPACTS OF USING LATENT ACTIVITIES FROM DIFFERENT LAYERS (%)

Layers	Size	Kappa	BAcc	WF1
All	6.9M	74.23 ± 1.36	75.57 ± 1.47	86.88 ± 0.66
First half	7.0M	62.97 ± 2.15	64.57 ± 1.54	81.00 ± 1.15
Second half	7.0M	<u>71.60 ± 1.14</u>	<u>68.40 ± 1.92</u>	<u>85.60 ± 0.52</u>
First quarter	6.9M	59.63 ± 2.49	58.75 ± 3.13	78.88 ± 1.43
Second quarter	6.9M	68.40 ± 2.66	<u>69.47 ± 1.45</u>	83.80 ± 1.35
Third quarter	6.9M	68.32 ± 1.22	64.39 ± 1.37	83.96 ± 0.63
Forth quarter	6.9M	<u>70.48 ± 2.21</u>	65.78 ± 1.46	<u>84.71 ± 1.16</u>

TABLE VI
IMPACTS OF DIFFERENT LATENT FUSION STRATEGIES (%)

Fusion	Size	Kappa	BAcc	WF1
Base	6.9M	74.23 ± 1.36	75.57 ± 1.47	86.88 ± 0.66
No	7.0M	61.60 ± 3.69	51.13 ± 7.15	79.93 ± 2.26
Mean	7.0M	<u>65.05 ± 1.41</u>	<u>59.40 ± 8.67</u>	<u>82.08 ± 0.83</u>

freezing pre-trained parameters is often preferable due to lower training costs and improved efficiency, while still demonstrating the ability to represent richer and more universal EEG features. Our method achieved performance comparable to, and in most cases exceeding, that of the second-best baseline, Gram-L, while being approximately 19× more lightweight.

B. Ablations

We examined the impacts of each component, reporting the mean and standard deviation of “kappa”, “BAcc”, and “WF1”.

1) *Signal Embedding and Noise Schedule of SSMDP*: Table II showed the impact of the μ -law, demonstrating the importance of handling the wide dynamic range of EEG. In Section III-B3b, we discussed the necessity of using a cosine noise schedule during the forward process. Here, we compared it with a diffusion model trained using the original linear noise schedule [10], followed by training a classifier on its latent activities. As shown in Table II, the linear noise schedule negatively impacted the classifier performance. Hence, cosine noise schedule was chosen.

2) *Latent Activities and Representations of SSMDP*: When extracting latent activities from SSMDP, we found that minimizing the effect of the diffusion forward process, by using a noiseless forward process and a small diffusion step, enhanced the quality of latent activities and consequently improved performance, as shown in Table II and Table III.

We also analyzed the performance of different latent activities of SSMDP and various pooling strategies. As shown in Table IV, when the pooling strategy is fixed, models using the latent activities of the gate channels outperformed those using other activities. Interestingly, standard deviation pooling, although rarely reported in the literature, outperformed average pooling, presumably because it better captured variability in time-series data.

3) *Latent Fusion through LFT*: While the convolution kernels of the bidirectional SSMDP captured global context (see Eq. (8)), it is worth investigating whether the layers in

TABLE VII
GENERALIZATION (%) OF SSMDP TRAINED ON TUEV TO UNSEEN DOWNSTREAM SEIZURES ON CHB-MIT, COMPARED WITH REPORTED WORKS IN [6].

Model	Size	BAcc	AUCPR	AUROC
<i>Training from Scratch on CHB-MIT (non-FM)</i>				
SPaRCNet [56]	0.79M	58.76 ± 1.91	12.47 ± 1.19	81.43 ± 1.48
ContraWR [57]	1.6M	63.44 ± 0.02	22.64 ± 1.74	80.97 ± 1.14
FFCL [58]	2.4M	62.62 ± 1.04	20.49 ± 3.46	82.71 ± 0.51
CNN-Trans [59]	3.2M	63.89 ± 0.67	24.79 ± 2.27	86.62 ± 0.82
ST-Trans [60]	3.5M	59.15 ± 1.95	14.22 ± 0.94	82.37 ± 4.91
<i>Pretrained with EEG Seizure Dataset (FM)</i>				
BIOT [1]	3.2M	70.68 ± 4.57	32.77 ± 4.60	87.61 ± 2.84
LaBraM-Base [2]	5.8M	70.75 ± 3.58	32.87 ± 4.02	86.79 ± 1.99
CBraMod [6]	4.0M	<u>73.98 ± 2.84</u>	<u>36.89 ± 3.82</u>	88.92 ± 1.54
<i>Pretrained without Seizure Dataset (non-FM)</i>				
EEGDM (Ours)	12.8M	83.79 ± 1.66	48.07 ± 1.17	<u>88.78 ± 0.37</u>

TABLE VIII
GENERALIZATION (%) EEGDM TO DIFFERENT SAMPLING RATE

Train	Test	Kappa	BAcc	WF1
200 Hz	200 Hz	74.23 ± 1.36	75.57 ± 1.47	86.88 ± 0.66
200 Hz	190 Hz	<u>70.26 ± 2.00</u>	<u>72.78 ± 1.38</u>	<u>85.17 ± 1.02</u>
200 Hz	180 Hz	66.54 ± 1.60	68.36 ± 2.07	83.38 ± 0.81

SSMDP still exhibit a hierarchical structure, where shallow layers capture local patterns and deep layers capture global, high-level patterns [52]. To examine the internal hierarchy of the proposed SSMDP, we trained LFT using only a fraction of the SSMDP’s layers. Since this reduced the size of the latent fusion module in LFT, the depth of the classification module was increased to compensate for the smaller model size. As shown in Table V, evaluation metrics generally improved when deeper layers were used, indicating that latent activities from deeper layers are more effective than those from earlier layers. Furthermore, incorporating latent activities from earlier layers in addition to deeper ones further improved performance.

We also explored two alternative methods with no trainable parameters: “no fusion”, where the EEG channel (C), layer (n) and pool (p) axes of latent tokens were simply flattened, and “mean fusion”, where latent fusion was performed by averaging along the layer (n) dimension. Since replacing latent fusion removed a substantial part of the latent fusion module, we increased the depth of the classification module to match the total number of trainable parameters in the base model for a fair ablation. The results in Table VI underscore the importance of our latent fusion.

C. Additional Analyses

1) *Generalization Beyond the Pretrained Dataset*: We investigated whether our SSMDP, pretrained on the TUEV dataset (without seizures), could generalize to an unseen downstream dataset collected from pediatric subjects with intractable seizures, namely CHB-MIT [22], which also differs in terms of the number of EEG channels (22 vs. 16), segment duration (5s vs. 10s), and the presence of class imbalance.

Despite these challenges, our method is flexible to handle any number of channels, and SSMDP can be directly applied to the first and second 5-second segments of CHB-MIT. LFT was fine-tuned on CHB-MIT with a simple class-balanced weighting based on class ratios on the loss function. We compared our performance with FMs previously evaluated on the same dataset, as summarized in Table VII. This comparison followed the experimental setup of [6] and utilized BAcc, the area under the precision-recall curve (AUPRC), and the area under the receiver operating characteristic curve (AUROC) as evaluation metrics. While FMs generally outperform models trained from scratch, it is noteworthy that existing FMs have been pretrained on seizure EEG data from either the same or different datasets. In contrast, our method, pretrained only on TUEV, demonstrated strong generalization, achieving superior performance across nearly all metrics.

2) *Generalization to Different Sampling Rates*: EEGDM preserved the time-continuous form of SSMs, enabling it to process EEG signals at different sampling rates. Table VIII presented the performance of models trained on data with a 200 Hz sampling rate and tested on data with different sampling rates. The results showed that performance degraded slightly but largely remained intact. Nevertheless, this capability is unique to the SSM-based method and not directly applicable to other EEG FMs.

VI. CONCLUSION AND FUTURE WORK

This work presented EEGDM, a diffusion-based framework for self-supervised EEG representation learning. EEGDM comprises a structured state-space model SSMDP trained with DDPM to capture temporal dynamics with high granularity and LFT for classification. Empirically, EEGDM achieved state-of-the-art performance on EEG event classification tasks when assessed using the TUEV dataset, despite having significantly fewer training samples and being approximately 19 \times smaller than current EEG FMs. Moreover, SSMDP generalized to unseen downstream CHB-MIT. Comprehensive ablation studies validated the effectiveness of each component. The findings suggested that EEGDM was a highly competitive alternative for EEG signal processing, particularly compared to FMs that relied on masking-based pretraining, which typically required large and diverse datasets to learn effective self-supervised representations.

While this study evaluated EEGDM on clinically relevant IED from TUEV and seizure from CHB-MIT, its potential generalizability to other EEG tasks is worth further investigation. Moreover, this work opened several other directions for future research. On one hand, it is valuable to further reduce the model size of the SSMDP and LTF while maintaining performance, for clinical practicality and efficiency. On the other hand, it is natural to explore the scalability and robustness of EEGDM as a new class of EEG FMs trained with diffusion processes and capable of leveraging diverse EEG and other biosignal datasets. Furthermore, recent advances in discrete diffusion models, which have shown promise in language models, represented another exciting direction worth exploring for EEG representation learning.

ACKNOWLEDGMENT

The work was supported by the Ministry of Higher Education Malaysia through the Fundamental Research Grant Scheme (FRGS/1/2023/ICT02/XMU/02/1), and Xiamen University Malaysia through Xiamen University Malaysia Research Fund (XMUMRF/2022-C10/IECE/0039, XMUMRF/2024-C13/IECE/0049).

REFERENCES

- [1] C. Yang, M. B. Westover, and J. Sun, “Biot: Biosignal transformer for cross-data learning in the wild,” in *Thirty-seventh Conference on Neural Information Processing Systems*, 2023. [Online]. Available: <https://openreview.net/forum?id=c2LZyTyddi>
- [2] W.-B. Jiang, L.-M. Zhao, and B.-L. Lu, “Large brain model for learning generic representations with tremendous EEG data in BCI,” in *The Twelfth International Conference on Learning Representations*, 2024. [Online]. Available: <https://openreview.net/forum?id=QzTpTRVtrP>
- [3] World Health Organization. (2024, Feb.) Epilepsy. [Accessed: 9-Aug-2025]. [Online]. Available: <https://www.who.int/news-room/fact-sheets/detail/epilepsy>
- [4] G. Wang, W. Liu, Y. He, C. Xu, L. Ma, and H. Li, “Eegpt: Pretrained transformer for universal and reliable representation of eeg signals,” *Advances in Neural Information Processing Systems*, vol. 37, pp. 39249–39280, 2024.
- [5] W.-B. Jiang, Y. Wang, B.-L. Lu, and D. Li, “NeuroLM: A universal multi-task foundation model for bridging the gap between language and EEG signals,” in *The Thirteenth International Conference on Learning Representations*, 2025. [Online]. Available: <https://openreview.net/forum?id=Io9yFt7XH7>
- [6] J. Wang, S. Zhao, Z. Luo, Y. Zhou, H. Jiang, S. Li, T. Li, and G. Pan, “CBramod: A criss-cross brain foundation model for EEG decoding,” in *The Thirteenth International Conference on Learning Representations*, 2025. [Online]. Available: <https://openreview.net/forum?id=NPNUHgHF2w>
- [7] Z. Li, W.-L. Zheng, and B.-L. Lu, “Gram: A large-scale general eeg model for raw data classification and restoration tasks,” in *ICASSP 2025-2025 IEEE International Conference on Acoustics, Speech and Signal Processing (ICASSP)*. IEEE, 2025, pp. 1–5.
- [8] D. Kostas, S. Aroca-Ouellette, and F. Rudzicz, “Bendr: Using transformers and a contrastive self-supervised learning task to learn from massive amounts of eeg data,” *Frontiers in Human Neuroscience*, vol. 15, p. 653659, 2021.
- [9] K. Yi, Y. Wang, K. Ren, and D. Li, “Learning topology-agnostic eeg representations with geometry-aware modeling,” *Advances in Neural Information Processing Systems*, vol. 36, pp. 53875–53891, 2023.
- [10] J. Ho, A. Jain, and P. Abbeel, “Denoising diffusion probabilistic models,” *Advances in neural information processing systems*, vol. 33, pp. 6840–6851, 2020.
- [11] A. Q. Nichol and P. Dhariwal, “Improved denoising diffusion probabilistic models,” in *International conference on machine learning*. PMLR, 2021, pp. 8162–8171.
- [12] Z. Kong, W. Ping, J. Huang, K. Zhao, and B. Catanzaro, “Diffwave: A versatile diffusion model for audio synthesis,” in *International Conference on Learning Representations*, 2020.
- [13] K. Goel, A. Gu, C. Donahue, and C. Ré, “It’s raw! audio generation with state-space models,” in *International conference on machine learning*. PMLR, 2022, pp. 7616–7633.
- [14] W. Xiang, H. Yang, D. Huang, and Y. Wang, “Denoising diffusion autoencoders are unified self-supervised learners,” in *Proceedings of the IEEE/CVF International Conference on Computer Vision*, 2023, pp. 15802–15812.
- [15] D. Baranchuk, A. Voynov, I. Rubachev, V. Khrulkov, and A. Babenko, “Label-efficient semantic segmentation with diffusion models,” in *International Conference on Learning Representations*, 2022.
- [16] S. Mukhopadhyay, M. Gwilliam, V. Agarwal, N. Padmanabhan, A. Swaminathan, S. Hegde, T. Zhou, and A. Shrivastava, “Diffusion models beat gans on image classification,” *arXiv preprint arXiv:2307.08702*, 2023.
- [17] S. Mukhopadhyay, M. Gwilliam, Y. Yamaguchi, V. Agarwal, N. Padmanabhan, A. Swaminathan, T. Zhou, J. Ohya, and A. Shrivastava, “Do text-free diffusion models learn discriminative visual representations?” in *European Conference on Computer Vision*. Springer, 2024, pp. 253–272.

[18] J. Huang, M. Li, and W. Chen, "Sad-ver: A self-supervised, diffusion probabilistic model-based data augmentation framework for visual-stimulus eeg recognition," *Advanced Engineering Informatics*, vol. 65, p. 103298, 2025.

[19] Y. Li, I. Y. Liao, N. Zhong, F. Toshihiro, Y. Wang, and S. Wang, "Generative ai enables the detection of autism using eeg signals," in *Chinese Conference on Biometric Recognition*. Springer, 2023, pp. 375–384.

[20] Y. Wang, S. Zhao, H. Jiang, S. Li, B. Luo, T. Li, and G. Pan, "Diffmdd: A diffusion-based deep learning framework for mdd diagnosis using eeg," *IEEE Transactions on Neural Systems and Rehabilitation Engineering*, vol. 32, pp. 728–738, 2024.

[21] A. Harati, M. Golmohammadi, S. Lopez, I. Obeid, and J. Picone, "Improved eeg event classification using differential energy," in *2015 IEEE Signal Processing in Medicine and Biology Symposium (SPMB)*. IEEE, 2015, pp. 1–4.

[22] J. Guttag, "Chb-mit scalp eeg database (version 1.0.0)," *PhysioNet*, 2010.

[23] F. Lotte and C. Guan, "Regularizing common spatial patterns to improve bci designs: Unified theory and new algorithms," *IEEE Transactions on Biomedical Engineering*, vol. 58, no. 2, pp. 355–362, 2011.

[24] Y. Song, Q. Zheng, B. Liu, and X. Gao, "Eeg conformer: Convolutional transformer for eeg decoding and visualization," *IEEE Transactions on Neural Systems and Rehabilitation Engineering*, vol. 31, pp. 710–719, 2022.

[25] S. K. Goh, H. A. Abbass, K. C. Tan, A. Al-Mamun, N. Thakor, A. Bezerianos, and J. Li, "Spatio-spectral representation learning for electroencephalographic gait-pattern classification," *IEEE Transactions on Neural Systems and Rehabilitation Engineering*, vol. 26, no. 9, pp. 1858–1867, 2018.

[26] H. Tang, S. Xie, X. Xie, Y. Cui, B. Li, D. Zheng, Y. Hao, X. Wang, Y. Jiang, and Z. Tian, "Multi-domain based dynamic graph representation learning for eeg emotion recognition," *IEEE Journal of Biomedical and Health Informatics*, vol. 28, no. 9, pp. 5227–5238, 2024.

[27] S. Tang, J. A. Dunnmon, K. Saab, X. Zhang, Q. Huang, F. Dubost, D. L. Rubin, and C. Lee-Messer, "Self-supervised graph neural networks for improved electroencephalographic seizure analysis," *arXiv preprint arXiv:2104.08336*, 2021.

[28] J. Xie, J. Zhang, J. Sun, Z. Ma, L. Qin, G. Li, H. Zhou, and Y. Zhan, "A transformer-based approach combining deep learning network and spatial-temporal information for raw eeg classification," *IEEE Transactions on Neural Systems and Rehabilitation Engineering*, vol. 30, pp. 2126–2136, 2022.

[29] E. Shi, S. Yu, Y. Kang, J. Wu, L. Zhao, D. Zhu, J. Lv, T. Liu, X. Hu, and S. Zhang, "Meet: A multi-band eeg transformer for brain states decoding," *IEEE Transactions on Biomedical Engineering*, vol. 71, no. 5, pp. 1442–1453, 2024.

[30] D.-Y. Lee, J.-H. Jeong, B.-H. Lee, and S.-W. Lee, "Motor imagery classification using inter-task transfer learning via a channel-wise variational autoencoder-based convolutional neural network," *IEEE transactions on neural systems and rehabilitation engineering*, vol. 30, pp. 226–237, 2022.

[31] D. Li, S. Huang, L. Xie, Z. Wang, and J. Xu, "Neuron perception inspired eeg emotion recognition with parallel contrastive learning," *IEEE Transactions on Neural Networks and Learning Systems*, 2025.

[32] H. Wang, P. Chen, M. Zhang, J. Zhang, X. Sun, M. Li, X. Yang, and Z. Gao, "Eeg-based motor imagery recognition framework via multi-subject dynamic transfer and iterative self-training," *IEEE Transactions on Neural Networks and Learning Systems*, vol. 35, no. 8, pp. 10 698–10 712, 2023.

[33] H.-Y. S. Chien, H. Goh, C. M. Sandino, and J. Y. Cheng, "Maeeg: Masked auto-encoder for eeg representation learning," in *NeurIPS 2022 Workshop on Learning from Time Series for Health*, 2022.

[34] C.-C. Chuang, C.-C. Lee, C.-H. Yeng, E.-C. So, B.-S. Lin, and Y.-J. Chen, "Convolutional denoising autoencoder based ssvep signal enhancement to ssvep-based bcis," *Microsystem Technologies*, vol. 28, no. 1, pp. 237–244, 2022.

[35] Y. Zhang, Y. Yu, H. Li, A. Wu, X. Chen, J. Liu, L.-L. Zeng, and D. Hu, "Dmae-eeg: A pretraining framework for eeg spatiotemporal representation learning," *IEEE Transactions on Neural Networks and Learning Systems*, 2025.

[36] M. H. Rafiei, L. V. Gauthier, H. Adeli, and D. Takabi, "Self-supervised learning for electroencephalography," *IEEE Transactions on Neural Networks and Learning Systems*, vol. 35, no. 2, pp. 1457–1471, 2022.

[37] A. Van Den Oord, O. Vinyals *et al.*, "Neural discrete representation learning," *Advances in neural information processing systems*, vol. 30, 2017.

[38] Y. Bengio, L. Yao, G. Alain, and P. Vincent, "Generalized denoising auto-encoders as generative models," *Advances in neural information processing systems*, vol. 26, 2013.

[39] A. C. Li, M. Prabhudesai, S. Duggal, E. Brown, and D. Pathak, "Your diffusion model is secretly a zero-shot classifier," in *Proceedings of the IEEE/CVF International Conference on Computer Vision*, 2023, pp. 2206–2217.

[40] K. Deja, T. Trzciński, and J. M. Tomczak, "Learning data representations with joint diffusion models," in *Joint European Conference on Machine Learning and Knowledge Discovery in Databases*. Springer, 2023, pp. 543–559.

[41] C.-S. Chen, S.-H. Chang, C.-W. Liu, and T.-M. Pan, "Exploring the potential of electroencephalography signal-based image generation using diffusion models: Integrative framework combining mixed methods and multimodal analysis," *JMIR Medical Informatics*, vol. 13, no. 1, p. e72027, 2025.

[42] D. Qi, L. Kong, L. Yang, and C. Li, "Audiodiffusion: Generating high-quality audios from eeg signals: Reconstructing audio from eeg signals," in *2023 4th International Symposium on Computer Engineering and Intelligent Communications (ISCEIC)*. IEEE, 2023, pp. 344–348.

[43] S. Kim, S.-H. Lee, Y.-E. Lee, J.-W. Lee, J.-H. Park, P. Kazanzides, and S.-W. Lee, "Brain-driven representation learning based on diffusion model," in *2024 12th International Winter Conference on Brain-Computer Interface (BCI)*. IEEE, 2024, pp. 1–4.

[44] T. Liu, Y. Qin, S. Zhang, and X. Tao, "A diffusion-based feature enhancement approach for driving behavior classification with eeg data," *Advanced Engineering Informatics*, vol. 65, p. 103279, 2025.

[45] B. B. Moser, A. S. Shanbhag, F. Raue, S. Frolov, S. Palacio, and A. Dengel, "Diffusion models, image super-resolution, and everything: A survey," *IEEE Transactions on Neural Networks and Learning Systems*, 2024.

[46] S. Wang, T. Zhou, Y. Shen, Y. Li, G. Huang, and Y. Hu, "Generative ai enables eeg super-resolution via spatio-temporal adaptive diffusion learning," *IEEE Transactions on Consumer Electronics*, 2025.

[47] X. Huang, C. Li, A. Liu, R. Qian, and X. Chen, "Eegdfus: a conditional diffusion model for fine-grained eeg denoising," *IEEE Journal of Biomedical and Health Informatics*, 2024.

[48] T. Salimans and J. Ho, "Progressive distillation for fast sampling of diffusion models," in *International Conference on Learning Representations*, 2022.

[49] O. Ronneberger, P. Fischer, and T. Brox, "U-net: Convolutional networks for biomedical image segmentation," in *Medical image computing and computer-assisted intervention–MICCAI 2015: 18th international conference, Munich, Germany, October 5–9, 2015, proceedings, part III 18*. Springer, 2015, pp. 234–241.

[50] A. Vaswani, N. Shazeer, N. Parmar, J. Uszkoreit, L. Jones, A. N. Gomez, Ł. Kaiser, and I. Polosukhin, "Attention is all you need," *Advances in neural information processing systems*, vol. 30, 2017.

[51] J. Ho and T. Salimans, "Classifier-free diffusion guidance," *arXiv preprint arXiv:2207.12598*, 2022.

[52] A. Gu, K. Goel, and C. Ré, "Efficiently modeling long sequences with structured state spaces," *arXiv preprint arXiv:2111.00396*, 2021.

[53] A. Gu, K. Goel, A. Gupta, and C. Ré, "On the parameterization and initialization of diagonal state space models," *Advances in Neural Information Processing Systems*, vol. 35, pp. 35 971–35 983, 2022.

[54] G. Chen, "Are electroencephalogram (eeg) signals pseudo-random number generators?" *Journal of Computational and Applied Mathematics*, vol. 268, pp. 1–4, 2014.

[55] I. Obeid and J. Picone, "The temple university hospital eeg data corpus," *Frontiers in neuroscience*, vol. 10, p. 196, 2016.

[56] J. Jing, W. Ge, S. Hong, M. B. Fernandes, Z. Lin, C. Yang, S. An, A. F. Struck, A. Herlopian, I. Karakis *et al.*, "Development of expert-level classification of seizures and rhythmic and periodic patterns during eeg interpretation," *Neurology*, vol. 100, no. 17, pp. e1750–e1762, 2023.

[57] C. Yang, D. Xiao, M. B. Westover, and J. Sun, "Self-supervised eeg representation learning for automatic sleep staging," *arXiv preprint arXiv:2110.15278*, 2021.

[58] H. Li, M. Ding, R. Zhang, and C. Xiu, "Motor imagery eeg classification algorithm based on cnn-lstm feature fusion network," *Biomedical signal processing and control*, vol. 72, p. 103342, 2022.

[59] W. Y. Peh, Y. Yao, and J. Dauwels, "Transformer convolutional neural networks for automated artifact detection in scalp eeg," in *2022 44th Annual International Conference of the IEEE Engineering in Medicine & Biology Society (EMBC)*. IEEE, 2022, pp. 3599–3602.

[60] Y. Song, X. Jia, L. Yang, and L. Xie, "Transformer-based spatial-temporal feature learning for eeg decoding," *arXiv preprint arXiv:2106.11170*, 2021.